Separation and Purification Technology 256 (2021) 117839

Contents lists available at ScienceDirect

Separation and Purification Technology

journal homepage: www.elsevier.com/locate/seppur

Low-pressure loose GO composite membrane intercalated by CNT for effective dye/salt separation

Lili Huang [a,b,c,1], Zhiying Li [a,b,1], Yang Luo [a,b,1], Ning Zhang [a,b,*], Wenxu Qi [a,b], En Jiang [a,b], Junjiang Bao [a,b], Xiaopeng Zhang [a,b], Wenji Zheng [a,b], Baigang An [c,*], Gaohong He [a,b,*]

[a] State Key Laboratory of Fine Chemicals, Dalian University of Technology, Dalian 116023, China
[b] School of Chemical Engineering, Dalian University of Technology, Panjin 124221, China
[c] School of Chemical Engineering, University of Science and Technology Liaoning, Anshan 114051, China

ARTICLE INFO

Keywords:
Loose GO film
CNT intercalation
Dye/salt separation
Nanofiltration

ABSTRACT

Low-pressure loose nanofiltration membranes were facilely fabricated by intercalating CNTs into graphene oxide (GO) laminates supported by cellulose acetate (CA) ultrafiltration substrates. The CNTs could loosen the GO laminar film and enlarge the interlayer spacing of GO laminates, thus reducing the resistance of water flux and salt permeation. Crosslinking bonds between GO layers were generated to create hydro-stable size-sieving channel necks of the tortuous pathway for selective molecular permeation. It was found that the GO composite membrane with 80 wt% of CNT content and 0.5 mg of GO loading exhibited the optimal separation performance in the application of textile wastewater treatment. It had the highest pure water permeability of 26.3 $L \cdot m^{-2} \cdot h^{-1} \cdot bar^{-1}$ and almost complete rejection to dyes (e.g. 98.7% for Congo red, 94.1% for Methyl blue) as well as the lowest rejections to salts (e.g. 3.1% for NaCl, 6.3% for Na_2SO_4) under a low transmembrane pressure of 1.0 bar. This work provides a feasible approach for designing GO-based membrane with improved dye/salt separation performance.

1. Introduction

Nowadays, synthetic dyes have been widely used in textile, printing, cosmetics, plastic and rubber products, etc. [1]. In conventional synthesis process, dyes are chemically produced followed by abundant by-products of inorganic salts (typically NaCl, Na_2SO_4). For example, acid blue 9 (a sulfonic acid substituted aromatic derivative, AB9) is initially synthesized by the condensation reaction in acid condition (e.g. HCl) and subsequently neutralized by NaOH. The added NaOH could react with HCl and the sulfonic acid group of AB9, producing NaCl and Na_2SO_4 mixed in the dye product [2,3]. Furthermore, the inorganic salts also stem from the dye purification by means of the salting-out method [4]. However, the residual salts in the dyes deteriorate the dyeability and stability of the dye products [5]. Therefore, it is in urgent need to seek an outstanding desalting method for obtaining high-quality and strong-stability dye suitable for practical applications.

There are several methods for dye desalination including oxidation, adsorption, coagulation/flocculation, etc. [3]. Oxidation is an energy-consuming method, limiting its wide application [3]. Adsorption is a popular and effective method for the salt removal from dyes, but the difficulty in the adsorbent regeneration or reactivation drastically lowers its adsorption performance [6]. In spite of the advantages of simple operation and low cost, the coagulation/flocculation method has difficulty in decolorizing the soluble dyes [7]. Compared with the traditional methods, membrane separation has received great attention in the removal of salinity in organic solution or wastewater due to the advantages of simple operation, high separation efficiency, and low energy consumption [8].

Among the membrane technologies, nanofiltration (NF) has been successfully applied to dye purification owing to the high rejection to low-molecular-weight (100–1000 Da) organic molecules, low operation pressure, relatively low operating and maintenance costs [9]. While the dense selective layer of common commercial NF membranes simultaneously rejects dyes and divalent salts (e.g. Na_2SO_4) [4,10]. This intrinsic drawback inevitably lowers the quality of the dye products and limits the application of NF membranes to dye purification. In this

* Corresponding authors at: State Key Laboratory of Fine Chemicals, Dalian University of Technology, Dalian 116023, China (N. Zhang and G. He).
E-mail addresses: zhangning@dlut.edu.cn (N. Zhang), baigang73@126.com (B. An), hgaohong@dlut.edu.cn (G. He).
[1] The authors have equal contribution to this work.

https://doi.org/10.1016/j.seppur.2020.117839
Received 14 June 2020; Received in revised form 31 August 2020; Accepted 4 October 2020
Available online 7 October 2020

regard, a small change in the structure of the selective layer of NF membrane is believed to improve the salt passage ability. Accordingly, loose NF membranes are emerging as a promising remedy for the dye/salts separation [11,12]. However, since most loose NF membranes are polymer composite membranes, several intrinsic deficiencies including weak chemical stability and poor antifouling ability limit their performance [13,14].

Recently, there has been a growing interest in the design of novel membranes based on ultrathin 2D materials such as GO [15,16], MoS_2 [17,18], MXene [19,20] and COF [20,21] nanosheets. Among these 2D materials, GO has gained increasing attention in membrane development due to its ultrathin thickness, hydrophilicity, strong mechanical strength, and good chemical stability [22]. Particularly, GO nanosheets contain plenty of oxygen-rich functional groups (hydroxyl, carboxyl, and epoxy groups) on the basal plane and at the lateral edges [23], which provide possible reactive sites for modification. The inherent properties of GO are more favored for membrane synthesis than pristine graphene. The thickness of layer-by-layer GO film is easily adjusted by depositing a different quantity of GO nanosheets [24], thereby conveniently tailoring the membrane performance [25]. The recently reported GO composite membranes with compact laminar structure exhibit excellent performance of high water permeance and rejection of dye and ions [26,27]. That is, pristine GO membrane with the effective channel size of 7.6 Å is permeable to water (i.e. 2.6 Å) [28], but impermeable to some hydrated divalent ions (e.g. Ca^{2+}, Mg^{2+}, and SO_4^{2-}) and dyes [29]. In order to achieve excellent dye/salt separation, the GO laminar layer needs to be further modified. Therefore, it is necessary to achieve a relatively loose GO laminar structure for enhancing the permeance of both water and ions and maintaining high rejection to dyes.

Doping nanoparticles is an effective method to obtain loose GO laminar film [30]. The enlarged interlayer spacing between GO nanosheets could enhance the membrane permeance to both water and salts [31]. Poly(sodium-p-styrenesulfonate) modified halloysite nanotubes were doped into the GO laminates to increase the interlayer spacing to 8.8 Å, thereby achieving a higher permeability of 8.8 $L \cdot m^{-2} \cdot h^{-1} \cdot bar^{-1}$ and effective separation of dyes and salts (i.e. the rejections follow 4.7% for $MgSO_4$, 4.7% for $MgCl_2$, 6.8% for NaCl, and 14.3% for Na_2SO_4, up to 97.9% for Reactive Black 5) [32]. Besides, GO/COF-1 nanocomposite membranes were synthesized by in-situ growth of COF-1 on GO surface, and the interlayer spacing of GO laminates increased to 10.3 Å [33]. The composite membrane showed excellent water permeation of 31 $L \cdot m^{-2} \cdot h^{-1} \cdot bar^{-1}$, high retention of water-soluble dyes (>99%) and low rejection to salts (<12%) [33]. Carbon nanotubes (CNTs) as an intercalation nanomaterial could enlarge the interlayer spacing of GO laminates. Zhang et al. [34] embedded oxidized CNTs (OCNTs) into the GO laminates via layer-by-layer self-assembly technique, producing the alternating sandwich structure of GO and OCNT. The intercalated OCNTs not only effectively increase the interlayer spacing to 17.7 Å, but also provide a new way for water transport. As the OCNT content increases from 0 to 80%, the zeta potential of the membrane varies from −18.7 to −49.2 mV. The negatively charged oxygen-containing groups of OCNT contribute to enhancing the Donnan effect of the membrane surface, which has negative effect on the rejection to ions. For the purpose of dye desalination, although the intercalation of OCNT into GO layers could facilitate water permeation, the ions would be retained in the feed side due to the enhanced Donnan effect of the introduced oxygen-containing functional groups on OCNT.

In order to enhance the membrane permeability to water and ions, we reported a novel strategy to expand the interlayer spacing of the GO laminates by intercalating non-oxidized CNTs into the GO laminates, which does not introduce the Donnan effect on ion permeation. The strategy not only expands the interlayer spacing of the GO laminates, but also permits free ion permeation through the GO laminates. Meanwhile, the expanded GO laminates were crosslinked by diamine molecules to create the size-sieving channel necks for selective molecular permeation. In this work, a series of CNT@GO composite membranes were fabricated by a facile pressurized filtration method. Cellulose acetate (CA) ultrafiltration membrane was selected as the support matrix due to its fruitful oxygen-containing groups for crosslinking the deposited GO laminates. With rational design, the layer-by-layer GO film intercalated by CNTs was obtained as schemed in Fig. 1. The expanded interlayer spacing could benefit the permeation of water and ions. Additionally, the size-sieving mechanism was proved for the dye/salt separation of the CNT@GO composite membranes.

2. Materials and methods

2.1. Materials

Natural graphite powder was purchased from Sinopharm Chemical Reagent Co., Ltd. Concentrated sulfuric acid (H_2SO_4, 98 wt%) was obtained from Beijing Chemical Works. Sodium nitrate ($NaNO_3$), sodium sulfate (Na_2SO_4), sodium chloride (NaCl), hydrogen peroxide (H_2O_2), Methyl blue (MB), Methylene blue (MB2) were provided by Tianjin Damao Chemical Reagent Factory. Meta-xylylenediamine (MXDA), Congo red (CR) and Fuchsin basic (FB) were obtained from Shanghai Aladdin. Carbon nanotubes (CNTs, ~15 nm) were purchased from Shenzhen Hongdachang Evolution Co., Ltd. Cellulose acetate film was purchased from Shanghai Xingya Purification Materials Factory. Deionized (DI) water was used in the experiment.

2.2. Preparation of CNT/GO dispersions

Modified Hummers method [35] was employed to synthesize GO nanosheets, which was subsequently purified by centrifugation at 8000 rpm for several times and dried at a temperature of 40 °C for 24 h. The prepared GO nanosheets were subjected to ultrasonication in DI water for 30 min for preparing a homogenous GO dispersion. The obtained GO dispersion was diluted to 0.02 mg/ml. Then 100 mg of MXDA serving as the crosslinking agent was added into 100 ml of the dilute GO dispersion. Simultaneously, a certain amount of CNTs were ultrasonically dispersed in DI water for 5 min under ice-water bath conditions. The obtained CNT dispersion was diluted to 0.02 mg/ml.

2.3. Preparation of CNT/GO composite membrane

Under ice-water bath conditions, the as-prepared GO dispersion (0.02 mg/ml) and CNT dispersion (0.02 mg/ml) were mixed with the CNT/GO weight ratio of 20, 40, 60, 80, 100 and 120% under ice-water bath conditions, producing the GO laminates with different CNT

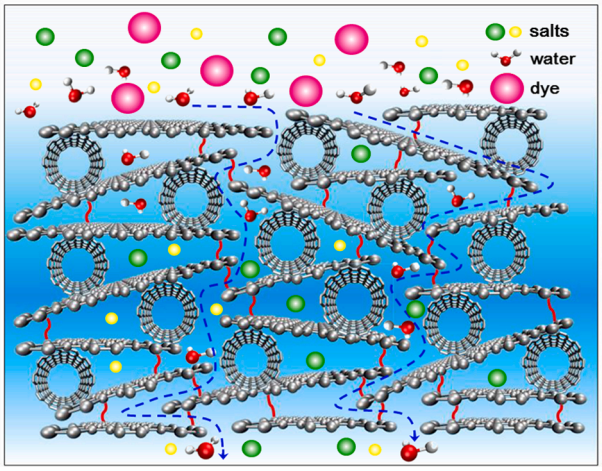

Fig. 1. The schematic structure of the CNT@GO composite membrane, in which the GO flakes are crosslinked by diamine molecules denoted by red solid lines.

contents. The CNT/GO weight ratio is defined as CNT content. Each CNT/GO mixture was ultrasonically mixed for 10 min, obtaining homogenous dispersion. CA ultrafiltration membrane with the average pore size of 0.1 μm was used as the supporting substrate for depositing the CNT@GO laminates. The CA substrate membrane has a circular shape with a diameter of 100 mm. The obtained CNT/GO dispersion was filtrated through the CA substrate via pressurized filtration method at room temperature, taking several hours to achieve the CNT@GO laminates. After the deposition, the CNT@GO laminates were crosslinked by MXDA in oven at 80 °C for one hour, producing the crosslinked CNT@GO (c-CNT@GO) membrane. Additionally, the composite membrane with pure GO laminates was also fabricated as the control sample. It was proved that the intercalated CNTs can effectively facilitate the permeation of water and ions, and maintain high rejection to dyes.

2.4. Material and composite membrane characterization

The morphology of the GO nanosheets and c-CNT@GO laminates was examined by a field emission scanning electron microscope (FESEM, Nova Nano SEM 450 from FEI, USA) and a transmission electron microscope (TEM, Tecnai G^2 F30 from FEI, USA). The molecular and crystal structures of the sample were characterized by Raman spectrometer (Raman, InVia from Renishaw, UK), Fourier transform infrared spectrometer (FTIR, Nicolet iN10 MX & iS10 from ThermoFisher, USA), X-ray photoelectron spectroscopy (XPS, ESCALABTM 250Xi from ThermoFisher, USA) and X-ray diffractometer (XRD, XRD-7000S from Shimadzu, Japan). The d-spacing of membrane laminates was calculated by the Bragg equation as follows:

$$2d\cdot\sin\theta = n\cdot\lambda \quad (1)$$

which d is the d-spacing of the composite membrane, θ is the diffraction angle, n indicates diffraction series is 1, λ is assigned to 0.154056 nm which represents the wave-length of the Cu X-ray beam.

2.5. Membrane filtration performance

The filtration performance of the c-CNT@GO composite membranes were characterized by testing the pure water permeability and the rejections to salts and dyes. The membranes were tested in a dead-end filtration cell with the effective membrane area of 10.17 cm^2. Prior to data sampling, each membrane was pressurized by DI water under 2.5 bar for 0.5 h to maintain a steady state. After that, the pressure was reduced to the operating pressure of 2.0 bar, producing a trans-membrane pressure difference of 1.0 bar. Then, the pure water permeability P_w ($L\cdot m^{-2}\cdot h^{-1}\cdot bar^{-1}$) was firstly measured at room temperature according to the following equation:

$$P_w = \frac{V}{A\cdot\Delta t\cdot\Delta P} \quad (2)$$

where V (L) is the volume of permeate water through the membrane, A (m^2) is the effective area of the membrane, Δt (h) means the permeation time, ΔP (bar) is the *trans*-membrane pressure.

To obtain the rejection properties of the c-CNT@GO composite membranes, the feed container was filled with aqueous solutions of dyes or salts. The rejection ratio (R) was estimated using the following equation:

$$R = (1-\frac{C_p}{C_f})\times 100\% \quad (3)$$

where C_p and C_f are the solute concentrations in the permeation and feed sides, respectively. The dye concentrations were determined by a UV–Vis spectrophotometer (UV-1700PC from Macy, China). The ion concentrations were determined by measuring the electrical As discussed above, the intercalation of CNTs conductivity of the aqueous solutions with a conductivity meter (DDS-307A from INESA, China). The dye solutions for test were prepared with the concentration of 0.1 g/L.

3. Results and discussion

Fig. 2(a) inset shows the TEM image of the prepared GO flakes with pleated, single-layered sheet-like structure. The oxygen-containing groups of GO were verified by FTIR spectroscopy as shown in Fig. 2a, the absorption peaks of C—O stretching (~1050 cm^{-1}), C—O—C stretching (~1270 cm^{-1}), C═C stretching (~1623 cm^{-1}), C═O stretching (~1726 cm^{-1}), and —OH stretching (~3300 cm^{-1}) are clearly observed in the pristine GO laminates, which are very consistent with the previous reports. Raman spectroscopy was also adopted to characterize the structure of the GO flakes. As shown in Fig. 2b, the Raman spectrum of GO exhibits a G band at 1596 cm^{-1} owing to the in-plane vibration of sp^2 carbon atom in graphite structure [36]. It also shows a D band at 1380 cm^{-1}, which indicates the presence of local defects/disorders in the GO powder such as vacancies, grain boundaries, bond-angle disorder, bond-length disorder, etc. [37]. The analysis of Raman spectrum shows the I_D/I_G ratio of 1.38. The high I_D/I_G ratio is associated with the formation of new sp^3 carbons in the graphite lattice [38], which increases the local defects/disorders of the GO flakes. The Raman spectrum confirms the fabrication of high oxidized GO flakes.

The chemical structure of CNT@GO and c-CNT@GO was further characterized by FTIR. As shown in Fig. 3, a new absorption peak is observed at a wavenumber of 1580 cm^{-1} in the c-CNT@GO membrane, corresponding to the stretching vibration of O═C—NH bonds [39]. This implies the success of the crosslinking reaction between GO and MXDA. Besides, the characteristic intensity of epoxy and carboxyl was notably

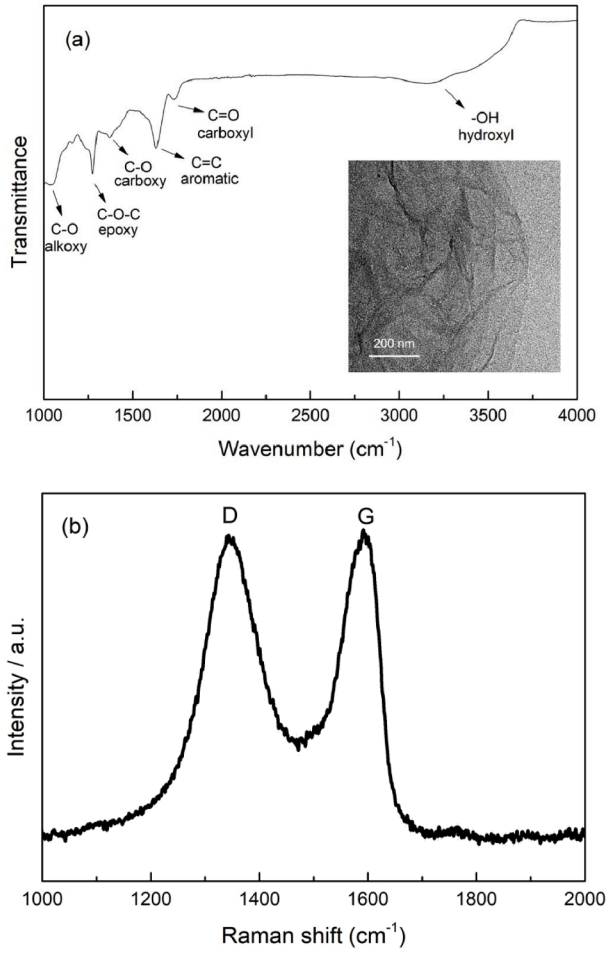

Fig. 2. Structure characterization of GO powder. (a) FTIR spectra with the inset of TEM spectra; (b) Representative Raman spectra.

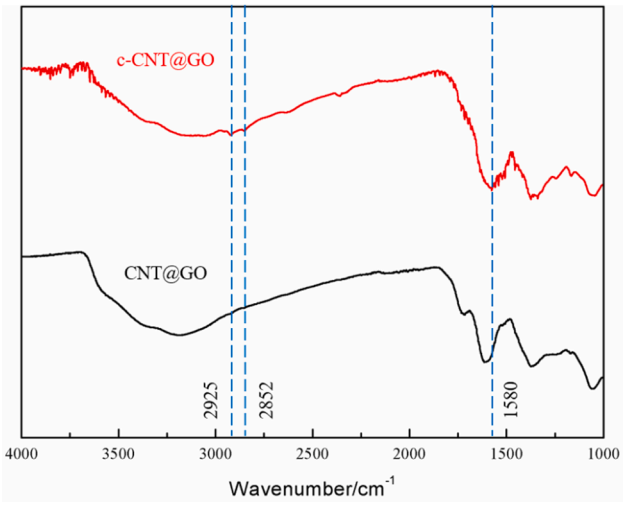

Fig. 3. FTIR spectra of CNT@GO and c-CNT@GO composite membranes.

reduced in the c-CNT@GO membrane, and new bands appear at the wavenumbers of 2925 and 2852 cm^{-1}, corresponding to the —CH_2— symmetric and asymmetric stretching of diamine molecules [40]. It further confirms the formation of the C—N covalent bonds via the condensation reaction between the amine groups of MXDA and the oxygen-containing groups of GO [41].

Fig. 4 shows the XPS analysis of the oxygen-containing functional groups of the c-CNT@GO composite membrane. As shown in Fig. 4(a), the C1s and O1s peaks were both observed in the pristine GO, CNT@GO and c-CNT@GO membranes. The pristine GO membrane exhibits the O/C ratio of 36%, while the CNT@GO membrane has a lower O/C ratio of 34%. It confirms that the CNTs are intercalated into the GO laminates, creating enlarged 3D nanochannels for enhancing its permeability to water. Besides, a new peak at 285.7 eV is observed in the c-CNT@GO membrane, corresponding to the C—N bonds formed by the crosslinking reaction. It further confirms the success of the crosslinking reactions between nearby GO nanosheets for enhancing the structural stability. After the crosslinking treatment, the O/C ratio of the CNT-intercalated GO laminates decreases from 34 to 29% due to the consumption of the oxygen-containing functional groups on the GO sheets in the cross-linking reactions with the diamine molecules [29]. Fig. 4(b)–(d) shows the deconvolution of the XPS C1s spectra of the pristine GO, CNT@GO and c-CNT@GO composite membranes. Four characteristic peaks are shown at the binding energies of around 284.3, 286.3, 287.2 and 288.4 eV, corresponding to C—C/C═C, C—O/C—O—C, C═O and O—C═O, respectively. As shown in Fig. 4(c), the intensity of the C-O-C peak is significantly reduced, while a new peak appears at 285.7 eV due to the formation of C-N bonds.

We observed the surface and cross-sectional morphology of the composite membrane by SEM. Fig. 5(a) and (b) show the pristine GO laminates with layered structure. It is shown in Fig. 5(c), (d) that the CNTs are well intercalated into the GO layers. The support of the intercalated CNTs will help maintain wide channel for water conduction. As shown in Fig. 6, the XRD patterns of the c-CNT@GO laminates reveal an intense feature diffraction peak at $2\theta = 9.4°$, corresponding to the interlayer spacing of 10.9 Å based on Eq. (1). It is known that the pristine GO laminates usually have the interlayer spacing in the range of 6–9 Å [42,43]. Therefore, the intercalation of CNTs could effectively increase the interlayer spacing of the GO laminates.

The performance of the c-CNT@GO composite membrane is shown in Fig. 7. Comparing with the pristine GO laminates, the c-CNT@GO membranes obviously exhibit lower rejection to salts of Na_2SO_4 and

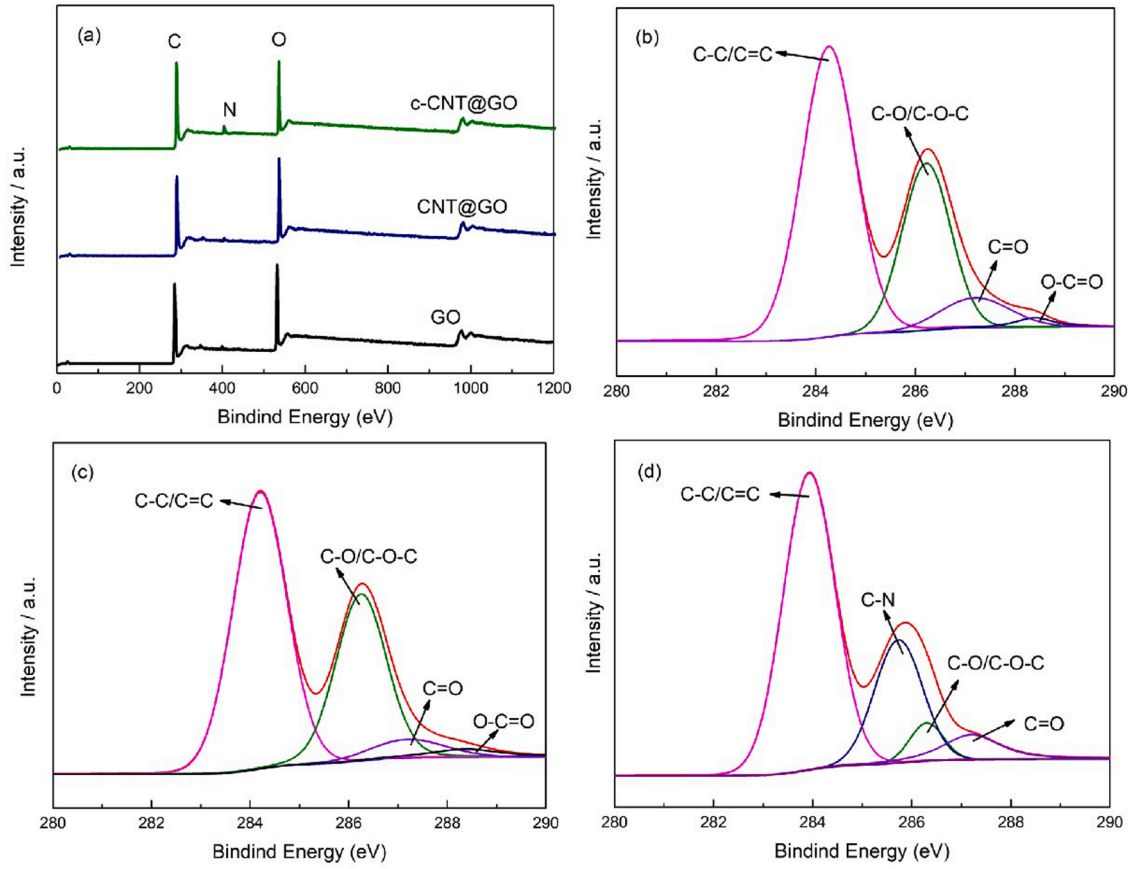

Fig. 4. XPS spectra with (a) wide scan of different materials and narrow scan for C1s peaks of (b) GO flakes, (c) CNT@GO and (d) c-CNT@GO composite membranes.

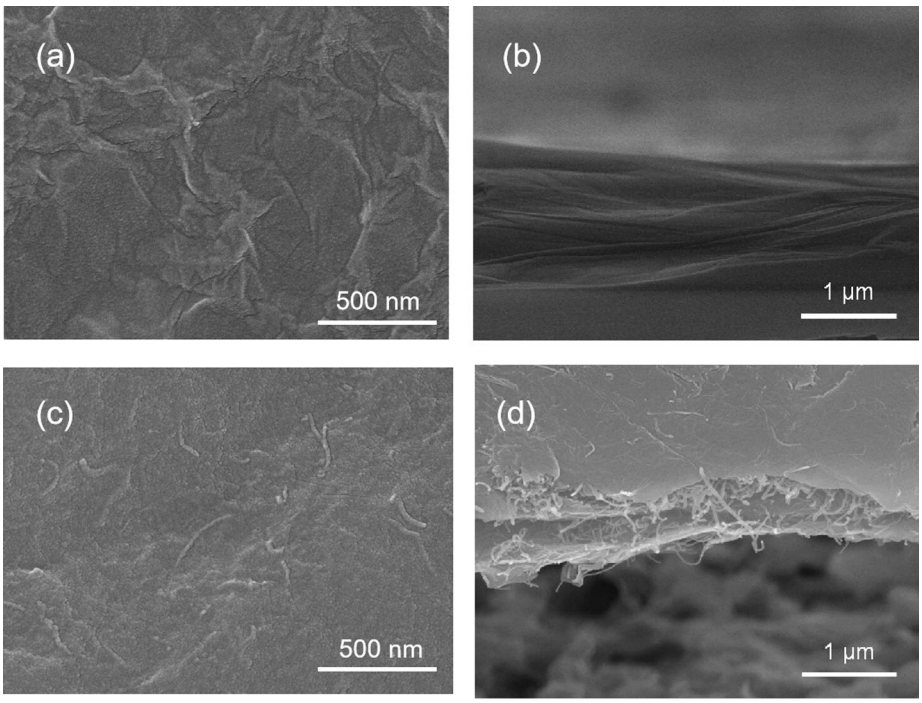

Fig. 5. Typical FESEM images: (a, b) Top-view and cross-section of pristine GO composite membrane; (c, d) Top-view and cross-section of c-CNT@GO composite membrane.

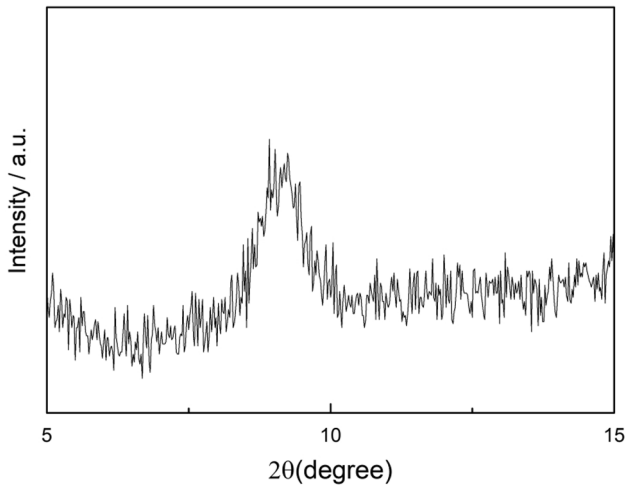

Fig. 6. XRD patterns of the GO laminates of the c-CNT@GO composite membrane.

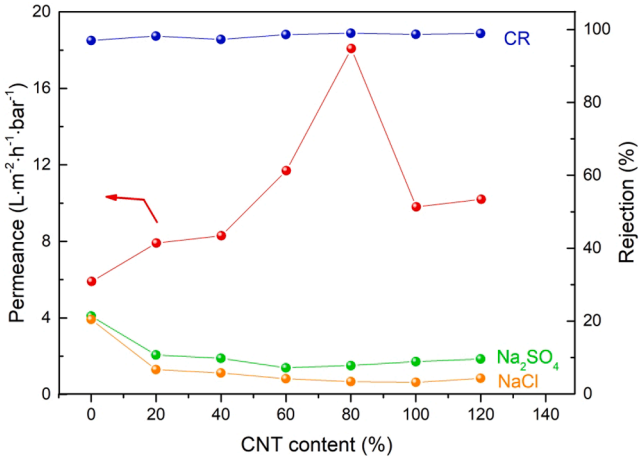

Fig. 7. Performance of c-CNT@GO membranes with different CNT contents.

NaCl. As CNTs were intercalated into the GO laminates, the rejections of Na_2SO_4 and NaCl both decrease from *ca.* 20% to 6.3 and 3.1%, respectively. Importantly, the crosslinking bonds between GO flakes could still maintain the narrow channel necks (Fig. 1) for rejecting the dye molecules. It is shown that the CNT intercalation has little impact on the dye rejection. The rejection of CR could maintain above 95% under various CNT contents. Thus the c-CNT@GO composite membranes have almost complete rejection to dye under different CNT contents. As the dye filtration tests evolve, the water permeance of the composite membranes exhibit a decreasing tendency within the initial period and then maintain stable, which is mainly due to the dye adsorption on the membrane surface. As CNTs are carbonaceous nanomaterials, the hydrophobic effects and π–π bonds endow CNTs with favorable adsorption capacity of dyes [44]. The partially exposed CNTs on the membrane surface could produce surface dye aggregation, blocking the nanoscale channels and thus reduce the water permeability. Therefore, future efforts should be paid on weakening the surface adsorption capacity of dyes by improving the chemical properties of the surface of c-CNT@GO membranes.

Fig. 7 also shows that as the CNT content increases, the water permeance of the membranes show an initially increasing and subsequently decreasing tendency. Under the CNT content of 80%, the composite membrane presents the highest water permeance of 18.28 $L{\cdot}m^{-2}{\cdot}h^{-1}{\cdot}bar^{-1}$. The intercalation of CNT loosens the GO laminates and greatly reduces the water flow resistance through the GO film. While under high CNT content, the π-π interaction between CNTs leads to the CNT aggregation in the GO laminates, which easily blocks the 2D channels and decreases the water permeance. As a result, the CNT content of 80% was determined in the preparation of the c-CNT@GO composite membrane, which is named as c-CNT@GO(80%).

Fig. 8 shows the effect of the thickness of CNT@GO layer on the pure water flux and rejections to dyes and salts. As shown in Fig. 8(a), the water flux keeps decreasing tendency as the GO loading increases. It

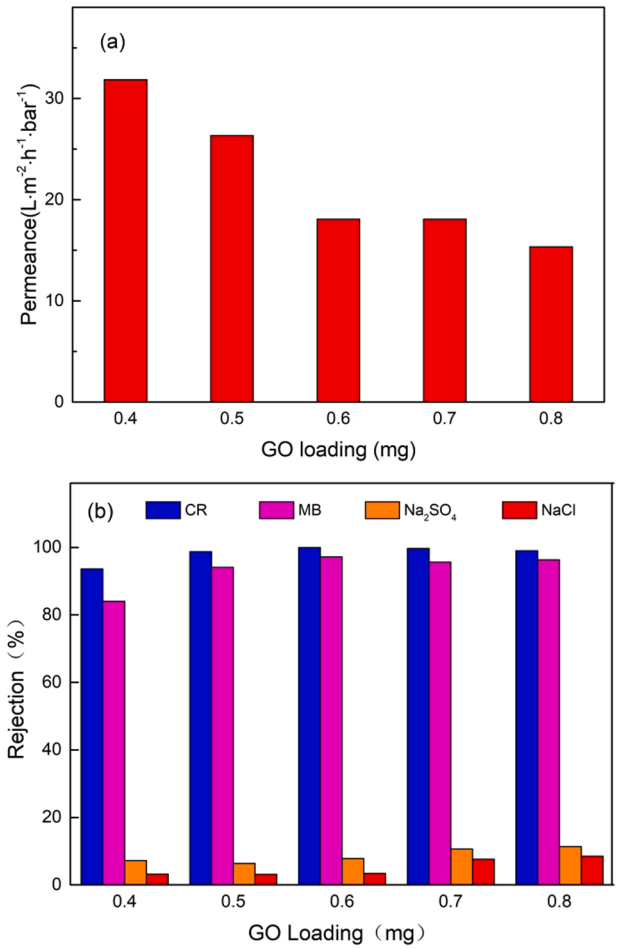

Fig. 8. Performance of the c-CNT@GO composite membranes with the CNT content of 80% as a function of GO loading. (a) Pure water flux; (b) rejections of dyes and ions.

clearly indicates that thicker CNT@GO layer leads to higher resistance to water permeation. In the interested range of GO loading, the flux decreases by almost half from 31.85 to 15.60 $L{\cdot}m^{-2}{\cdot}h^{-1}{\cdot}bar^{-1}$. As the CNT@GO thickness increases, the rejections to CR and MB increases and maintains above 95% under the GO loading of 0.5 mg, while the rejections to NaCl and Na_2SO_4 gradually increase to 8.5 and 11.3%, respectively. Accordingly, the c-CNT@GO composite membrane with the CNT content of 80% and GO loading of 0.5 mg, named as c-CNT@GO (80%, 0.5 mg), could achieve the dye/salt performance of a high water flux of 26.3 $L{\cdot}m^{-2}{\cdot}h^{-1}{\cdot}bar^{-1}$ and almost complete rejection to CR and MB (>94%) as well as very low salt retention of 3.1% for NaCl and 6.3% for Na_2SO_4 at a low operating pressure of 1 bar. The good-performance membrane is believed to be applicable to dye desalination. Table 1 shows the comparisons of the c-CNT@GO(80%, 0.5 mg) membrane performance with other loose NF membranes [9,14,45,46]. These results demonstrate that the c-CNT@GO(80%, 0.5 mg) membrane exhibits high dye rejection and salt penetration with relatively high water permeance. As discussed above, the intercalation of CNTs effectively loosens the GO laminates and the diamine crosslinkers helps to maintain the narrow necks along the permeating pathway, enhancing the permeance of water and salts and maintaining high dye rejection.

Fig. 9 summaries the dye rejections of the c-CNT@GO(80%, 0.5 mg) membranes varying with the molecular weight of dye. The dye rejection approximately follows the order of the molecular weight of dye. The relatively higher-molecular-weight dyes, such as CR ($M_w = 697$) and MB ($M_w = 800$), show higher rejections of 98.7% and 94.1%, respectively; while the lower-molecular-weight dyes, such as FB ($M_w = 301$) and MB2

Table 1
Comparison of the performance of the NF membranes.

Membrane	Pure water flux ($L{\cdot}m^{-2}{\cdot}h^{-1}{\cdot}bar^{-1}$)	Dye rejection (%)	Salt rejection (%)	Ref.
GO/NH_2-FE_3O_4	78.0	CR: 94.0	NaCl: 15	[45]
PAN/GO	33.0	MB: 100 AR: 99.8	NaCl: 10.9	[14]
LDHs/PEI	19.86	MB: 97.9 AF: 97.5	NaCl: 3	[47]
EGC/PEI	19.0	CR: 99.0	Na_2SO_4: 4.1	[9]
MoS_2-PSBMA	18.05	RB5: 98.2 RG19: 99.3	Na_2SO_4: 2.2 NaCl: 1.1	[48]
PDA-$FeCl_3$/H_2O_2	17.5	CR: 99.0 RB2: 98.2	NaCl: 5.6	[49]
TFC	16.8	BB: >99.7	Na_2SO_4: 11.6 NaCl: 3.4	[46]
c-CNTs@GO	26.3	CR: 98.7 MB: 94.1	Na_2SO_4: 6.3 NaCl: 3.1	This work

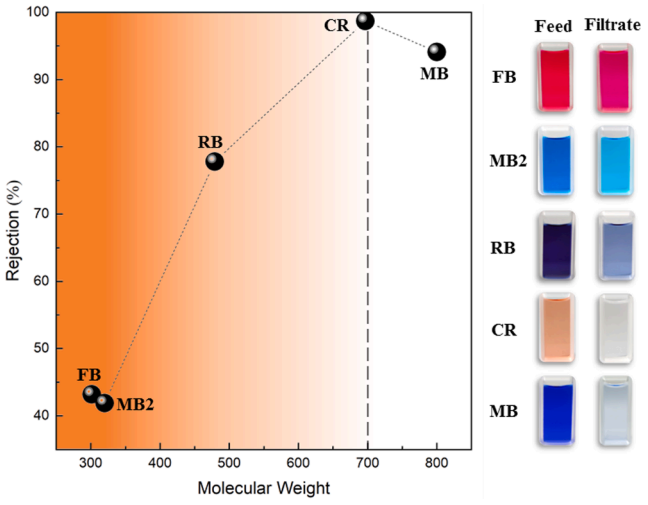

Fig. 9. Dye rejections of c-CNT@GO(80%, 0.5 mg) membrane as a function of molecular weight of dye. The right panel shows the image of the feed solution and collected filtrate.

($M_w = 320$), only exhibit the rejections of 43.2% and 41.9%, respectively; and a moderate rejection (e.g. 77.8%) is observed for RB ($M_w = 479$) with the molecular weight between them. It was reported that CR molecules tended to aggregate in aqueous solutions via π-π stacking interactions [45,46]. As a result, the GO composite membrane shows more efficient rejection to CR due to the larger size of the dye aggregates. According to the dependence of dye rejection on molecular size, it is suggested that the fabricated membranes have the size-sieving ability to purify the dyes from aqueous solutions.

4. Conclusion

A loose GO composite membrane was designed and facilely fabricated by co-deposition of graphene oxide (GO) and carbon nanotube (CNT) onto CA ultrafiltration substrate. Diamine molecules were used to stabilize the loosely stacked GO laminates in aqueous solutions and maintain the size-sieving channel necks via the crosslinking reaction between adjacent GO nanosheets. The characterization of the c-CNT@GO composite membrane by SEM, XPS, and XRD showed that the loosely stacked GO laminates were well constructed. The effect of CNT/GO ratio on the separation performance of membrane was studied. It was discovered that the intercalation of CNTs could loosen the GO

laminar film, thus enlarging the interlayer spacing of GO sheets and reducing the resistance of water flux and salt permeation. When the CNT content was 80%, the c-CNT@GO composite membrane exhibited the optimized dye/salt separation performance under a low operating pressure of 1.0 bar, where the pure water permeability was 26.3 $L{\cdot}m^{-2}{\cdot}h^{-1}{\cdot}bar^{-1}$, the rejections of CR and MB were 98.7 and 94.1%, and retentions of NaCl and Na_2SO_4 were only 3.1 and 6.3%. This illustrates that the novel membranes designed in this paper have potential for the separation of dye/salt mixtures in textile wastewater.

Declaration of Competing Interest

The authors declare that they have no known competing financial interests or personal relationships that could have appeared to influence the work reported in this paper.

Acknowledgements

This research has been supported by National Natural Science Foundation of China (Grant Nos. U1808209, 21506019), the Fundamental Research Funds for the Central Universities (Grant Nos. DUT20JC43, DUT19TD33), the Program for Changjiang Scholars (T2012049).

References

[1] J. Abdi, M. Vossoughi, N.M. Mahmoodi, I. Alemzadeh, Synthesis of metal-organic framework hybrid nanocomposites based on GO and CNT with high adsorption capacity for dye removal, Chem. Eng. J. 326 (2017) 1145–1158.
[2] J. Zhu, M. Tian, J. Hou, J. Wang, J. Lin, Y. Zhang, J. Liu, B. Van der Bruggen, Surface zwitterionic functionalized graphene oxide for a novel loose nanofiltration membrane, J. Mater. Chem. A 4 (5) (2016) 1980–1990.
[3] C. Xue, Q. Chen, Y.-Y. Liu, Y.-L. Yang, D. Xu, L. Xue, W.-M. Zhang, Acid blue 9 desalting using electrodialysis, J. Membr. Sci. 493 (2015) 28–36.
[4] Q. Zhang, L. Fan, Z. Yang, R. Zhang, Y.-N. Liu, M. He, Y. Su, Z. Jiang, Loose nanofiltration membrane for dye/salt separation through interfacial polymerization with in-situ generated TiO2 nanoparticles, Appl. Surf. Sci. 410 (2017) 494–504.
[5] J. Huang, K. Zhang, The high flux poly (m-phenylene isophthalamide) nanofiltration membrane for dye purification and desalination, Desalination 282 (2011) 19–26.
[6] C.-Z. Liang, S.-P. Sun, F.-Y. Li, Y.-K. Ong, T.-S. Chung, Treatment of highly concentrated wastewater containing multiple synthetic dyes by a combined process of coagulation/flocculation and nanofiltration, J. Membr. Sci. 469 (2014) 306–315.
[7] M. Riera-Torres, C. Gutiérrez-Bouzán, M. Crespi, Combination of coagulation–flocculation and nanofiltration techniques for dye removal and water reuse in textile effluents, Desalination 252 (1–3) (2010) 53–59.
[8] N. Mohammadi, H. Khani, V.K. Gupta, E. Amereh, S. Agarwal, Adsorption process of methyl orange dye onto mesoporous carbon material-kinetic and thermodynamic studies, J. Colloid Interface Sci. 362 (2) (2011) 457–462.
[9] N. Zhang, B. Jiang, L. Zhang, Z. Huang, Y. Sun, Y. Zong, H. Zhang, Low-pressure electroneutral loose nanofiltration membranes with polyphenol-inspired coatings for effective dye/divalent salt separation, Chem. Eng. J. 359 (2019) 1442–1452.
[10] R. Zhang, Y. Liu, M. He, M. Wu, Z. Jiao, Y. Su, Z. Jiang, P. Zhang, X. Cao, Mussel-inspired construction of organic-inorganic interfacial nanochannels for ion/organic molecule selective permeation, J. Membr. Sci. 555 (2018) 337–347.
[11] L. Yu, Y. Zhang, H. Zhang, J. Liu, Development of a molecular separation membrane for efficient separation of low-molecular-weight organics and salts, Desalination 359 (2015) 176–185.
[12] J. Zhu, M. Tian, Y. Zhang, H. Zhang, J. Liu, Fabrication of a novel "loose" nanofiltration membrane by facile blending with Chitosan-Montmorillonite nanosheets for dyes purification, Chem. Eng. J. 265 (2015) 184–193.
[13] J. Zhu, A. Uliana, J. Wang, S. Yuan, J. Li, M. Tian, K. Simoens, A. Volodin, J. Lin, K. Bernaerts, Y. Zhang, B. Van der Bruggen, Elevated salt transport of antimicrobial loose nanofiltration membranes enabled by copper nanoparticles via fast bioinspired deposition, J. Mater. Chem. A 4 (34) (2016) 13211–13222.
[14] Z. Qiu, X. Ji, C. He, Fabrication of a loose nanofiltration candidate from Polyacrylonitrile/Graphene oxide hybrid membrane via thermally induced phase separation, J Hazard Mater 360 (2018) 122–131.
[15] J. Abraham, K.S. Vasu, C.D. Williams, K. Gopinadhan, R.R. Nair, Tunable sieving of ions using graphene oxide membranes, Nature 12 (6) (2017) 546–550.
[16] C. Chen, Q.-H. Yang, Y. Yang, W. Lv, Y. Wen, P.-X. Hou, M. Wang, H.-M. Cheng, Self-assembled free-standing graphite oxide membrane, Adv. Mater. 21 (29) (2009) 3007–3011.
[17] K.F. Mak, K. He, C. Lee, G.H. Lee, J. Hone, T.F. Heinz, J. Shan, Tightly bound trions in monolayer MoS2, Nat. Mater. 12 (3) (2012) 207–211.
[18] S. Wu, Z. Zeng, Q. He, Z. Wang, S.J. Wang, Y. Du, Z. Yin, X. Sun, W. Chen, H. Zhang, Electrochemically reduced single-layer MoS(2) nanosheets: characterization, properties, and sensing applications, Small 8 (14) (2012) 2264–2270.
[19] J. Wang, P. Chen, B. Shi, W. Guo, M. Jaroniec, S.Z. Qiao, A regularly channeled lamellar membrane for unparalleled water and organics permeation, Angew. Chem. Int. Ed. Engl. 57 (23) (2018) 6814–6818.
[20] X. Wu, X. Cui, W. Wu, J. Wang, Y. Li, Z. Jiang, Elucidating ultrafast molecular permeation through well-defined 2D nanochannels of lamellar membranes, Angew. Chem. Int. Ed. Engl. 58 (2019) 18524–18529.
[21] W. Zhang, L. Zhang, H. Zhao, B. Li, H. Ma, A two-dimensional cationic covalent organic framework membrane for selective molecular sieving, J. Mater. Chem. A 6 (27) (2018) 13331–13339.
[22] S. Bano, A. Mahmood, S.-J. Kim, K.-H. Lee, Graphene oxide modified polyamide nanofiltration membrane with improved flux and antifouling properties, J. Mater. Chem. A 3 (5) (2015) 2065–2071.
[23] Y. Ying, Y. Yang, W. Ying, X. Peng, Two-dimensional materials for novel liquid separation membranes, Nanotechnology 27 (33) (2016) 1–28.
[24] S. Wei, Y. Xie, Y. Xing, L. Wang, H. Ye, X. Xiong, S. Wang, K. Han, Two-dimensional graphene Oxide/MXene composite lamellar membranes for efficient solvent permeation and molecular separation, J. Membr. Sci. 582 (2019) 414–422.
[25] J.G. Liu, T.S. Zhao, Z.X. Liang, R. Chen, Effect of membrane thickness on the performance and efficiency of passive direct methanol fuel cells, J. Power Sources 153 (1) (2006) 61–67.
[26] Y. Zhang, S. Zhang, J. Gao, T.-S. Chung, Layer-by-layer construction of graphene oxide (GO) framework composite membranes for highly efficient heavy metal removal, J. Membr. Sci. 515 (2016) 230–237.
[27] Q. Nan, P. Li, B. Cao, Fabrication of positively charged nanofiltration membrane via the layer-by-layer assembly of graphene oxide and polyethylenimine for desalination, Appl. Surf. Sci. 387 (2016) 521–528.
[28] D. Suresh, P.C. Nethravathi, Udayabhanu, H. Nagabhushana, S.C. Sharma, Spinach assisted green reduction of graphene oxide and its antioxidant and dye absorption properties, Ceram. Int. 41 (3) (2015) 4810–4813.
[29] N. Zhang, W. Qi, L. Huang, E. Jiang, J. Bao, X. Zhang, B. An, G. He, Review on structural control and modification of graphene oxide-based membranes in water treatment: From separation performance to robust operation, Chin. J. Chem. Eng. 27 (6) (2019) 1348–1360.
[30] Y. Han, Y. Jiang, C. Gao, High-flux graphene oxide nanofiltration membrane intercalated by carbon nanotubes, ACS Appl. Mater. Interfaces 7 (15) (2015) 8147–8155.
[31] Y. Huang, Q. Wei, Y. Wang, L. Dai, Three-dimensional amine-terminated ionic liquid functionalized graphene/Pd composite aerogel as highly efficient and recyclable catalyst for the Suzuki cross-coupling reactions, Carbon 136 (2018) 150–159.
[32] L. Zhu, H. Wang, J. Bai, J. Liu, Y. Zhang, A porous graphene composite membrane intercalated by halloysite nanotubes for efficient dye desalination, Desalination 420 (2017) 145–157.
[33] X. Zhang, H. Li, J. Wang, D. Peng, J. Liu, Y. Zhang, In-situ grown covalent organic framework nanosheets on graphene for membrane-based dye/salt separation, J. Membr. Sci. 581 (2019) 321–330.
[34] H. Zhang, X. Quan, S. Chen, X. Fan, G. Wei, H. Yu, Combined effects of surface charge and pore size on Co-enhanced permeability and ion selectivity through RGO-OCNT nanofiltration membranes, Environ. Sci. Technol. 52 (8) (2018) 4827–4834.
[35] William S. Hummers Jr., R.E. Offeman, Preparation of graphitic oxide, J. Am. Chem. Soc. 80 (6) (1958) 1339.
[36] A.C. Ferrari, J.C. Meyer, V. Scardaci, C. Casiraghi, M. Lazzeri, F. Mauri, S. Piscanec, D. Jiang, K.S. Novoselov, S. Roth, A.K. Geim, Raman spectrum of graphene and graphene layers, Phys. Rev. Lett. 97 (18) (2006), 187401.
[37] K. Krishnamoorthy, M. Veerapandian, K. Yun, S.J. Kim, The chemical and structural analysis of graphene oxide with different degrees of oxidation, Carbon 53 (2013) 38–49.
[38] A.C. Ferrari, J. Robertson, Interpretation of Raman spectra of disordered and amorphous carbon, Phys. Rev. B 61 (2000) 14095–14107.
[39] W.-S. Hung, C.-H. Tsou, M. De Guzman, Q.-F. An, Y.-L. Liu, Y.-M. Zhang, C.-C. Hu, K.-R. Lee, J.-Y. Lai, Cross-linking with diamine monomers to prepare composite graphene oxide-framework membranes with varying d-spacing, Chem. Mater. 26 (9) (2014) 2983–2990.
[40] J. Cai, J. Chen, P. Zeng, Z. Pang, X. Kong, Molecular mechanisms of CO2 adsorption in diamine-cross-linked graphene oxide, Chem. Mater. 31 (10) (2019) 3729–3735.
[41] N. Zhang, W. Qi, L. Huang, E. Jiang, Z. Li, Y. Luo, X. Zhang, J. Bao, W. Zheng, G. He, A composite membrane of cross-linked GO network semi-interpenetrating in polysulfone substrate for dye removal from water, J. Membr. Sci. 613 (2020), 118456.
[42] J. Sun, C. Hu, Z. Liu, H. Liu, J. Qu, Surface charge and hydrophilicity improvement of graphene membranes via modification of pore surface oxygen-containing groups to enhance permeability and selectivity, Carbon 145 (2019) 140–148.
[43] Z. Luo, Q. Fang, X. Xu, D.V. Raj, X. Zhou, Z. Liu, Attapulgite nanofibers and graphene oxide composite membrane for high-performance molecular separation, J. Colloid Interface Sci. 545 (2019) 276–281.
[44] K.B. Tan, M. Vakili, B.A. Horri, P.E. Poh, A.Z. Abdullah, B. Salamatinia, Adsorption of dyes by nanomaterials: recent developments and adsorption mechanisms, Sep. Purif. Technol. 150 (2015) 229–242.

[45] L. Dong, M. Li, S. Zhang, X. Si, Y. Bai, C. Zhang, NH2-Fe3O4-regulated graphene oxide membranes with well-defined laminar nanochannels for desalination of dye solutions, Desalination 476 (2020) 1–11.
[46] F. Soyekwo, C. Liu, H. Wen, Y. Hu, Construction of an electroneutral zinc incorporated polymer network nanocomposite membrane with enhanced selectivity for salt/dye separation, Chem. Eng. J. 380 (2020), 122560.
[47] S. Zhao, H. Zhu, Z. Wang, P. Song, M. Ban, X. Song, A loose hybrid nanofiltration membrane fabricated via chelating-assisted in-situ growth of Co/Ni LDHs for dye wastewater treatment, Chem. Eng. J. 353 (2018) 460–471.
[48] X. Liang, P. Wang, J. Wang, Y. Zhang, W. Wu, J. Liu, B. Van der Bruggen, Zwitterionic functionalized MoS2 nanosheets for a novel composite membrane with effective salt/dye separation performance, J. Membr. Sci. 573 (2019) 270–279.
[49] J. Zhu, M.T. Tsehaye, J. Wang, A. Uliana, M. Tian, S. Yuan, J. Li, Y. Zhang, A. Volodin, B. Van der Bruggen, A rapid deposition of polydopamine coatings induced by iron (III) chloride/hydrogen peroxide for loose nanofiltration, J. Colloid Interface Sci. 523 (2018) 86–97.